Supplementary Information

Speckle Tweezers for Manipulation of High and Low Refractive Index Micro-particles and Nano-particle Loaded Vesicles

Ramin Jamali[1], Farzaneh Nazari[2], Azadeh Ghaffari[3], Sabareesh K. P. Velu[4], Ali-Reza Moradi[1,5,*]

[1] Department of Physics, Institute for Advanced Studies in Basic Sciences (IASBS), Zanjan 45137-66731, Iran

[2] Department of Physics, Yazd University, Yazd 89195-741, Iran

[3] Department of Food and Drug Control, School of Pharmacy, Zanjan University of Medical Sciences, Zanjan 45139-56111, Iran

[4] Department of Physics, Rathinam College of Arts and Science, Coimbatore 641021, Tamilnadu, India

[5] School of Nano Science, Institute for Research in Fundamental Sciences (IPM), Tehran 19395-5531, Iran

[*]Corresponding author: *moradika@iasbs.ac.ir*

Figures and Tables Contents:

Videos Contents:

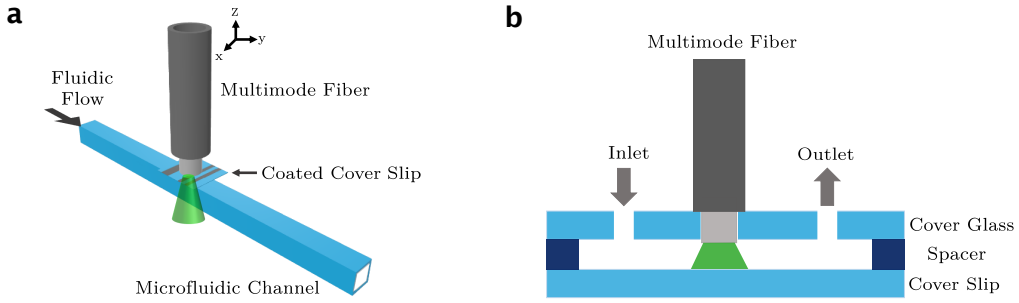

Supplementary Fig. S 1: Schematic of sample chambers for (a) flowing and (b) quiescent fluid.

For the experiments involving flow through microfluidic channels we used square cross-section capillaries with a 500 μm×500 μm inner pathway (Fig. S1**a**). These capillaries are purchased from VitroCom. We added the manufacturer information to the text. In these special chambers parts of the upper building walls are coated by a semi-transparent thin layer.

In Fig. S1**b** the sketch of the sample chamber that we fabricated for the experiments in which the fiber end is positioned inside the sample through making a hole on the cover glass. The fiber end is mounted on a gimbal mount on a xyz-micropositioner. Therefore, its position and angle can be aligned and controlled for the experiments. The fiber can be axially moved toward or away of the chamber. The cover glass includes also an inlet-outlet to inject or withdraw the fluidic sample. This cover glass is sticked to a cover slip by a double sided scotch.

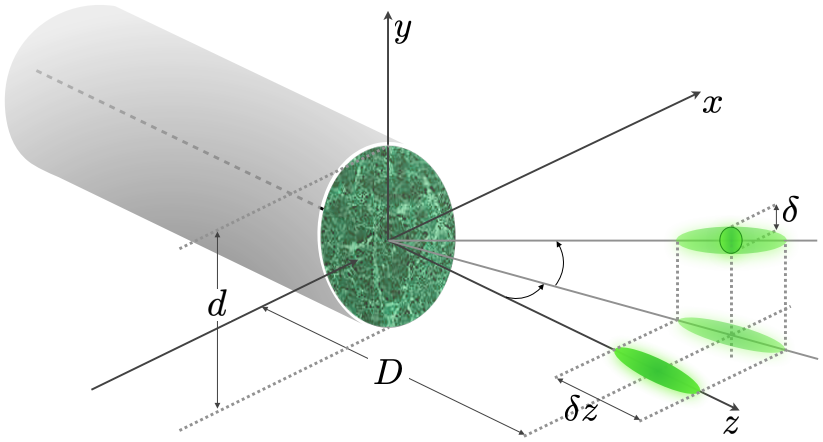

Supplementary Fig. S 2: Speckle grain size calculation in lateral and axial directions.

Depending on how speckles were created (scattering from a reflective rough surface, through a translucent matter, or mode-mixing in a multimode fiber) and how are being observed (the detector distance and the possible inclusion of an imaging lens), different parameters may characterize the field and define the speckle field properties such as grain size, contrast, correlation, etc. Diffraction is the optical phenomenon behind this conclusion. Basically, the speckle field can be formed by the use of any sufficiently coherent light source. Taking into account the size of the particles subjected to manipulation by the speckle field the required grain size may be considered. The adjustment can be performed either by the wavelength or the geometry of the optical system. In our manuscript, considering the particles typical size, the use of multimode fiber (the allowed number of propagating modes) and the possibility to change the fiber-sample distance, and also the availability

of the laser sources, we performed our experiments with a 532 nm laser.
In the following the dependence of the grain size on the wavelength and the geometry of the speckle generating system is discussed. Further details can be found in [1,2].

For calculation of the lateral size of a speckle grain consider a subjective speckle pattern generation in which different point sources on the diffusive object are imaged into adjacent points on the image plane distanced by D from the system aperture. If the emerging wavelets are in phase at a point they create a constructive interference hence a bright spot. If we now consider another point located at the same image plane but laterally displaced by a small distance (y), the arrived wavelets will present some phase difference. The maximum phase difference will occur between points located at opposite extremes of the aperture of the system, and the corresponding path difference can be evaluated as $\Delta = d \sin\theta$, where d is the system aperture diameter and θ the angle defined by the optical axis and the line going from the center of the system to the point image. In order to ensure that the point image and the displaced image do not differ significantly from the diffraction point of view, it is necessary that the path difference remain much smaller than the wavelength λ: $d\frac{y}{D} \ll \lambda$. The lateral extension δ or diameter of the bright spot at the imaging point, which can be taken as the "typical size" a single speckle grain, can now be defined as:

$$\delta = 2y \approx 2\lambda\frac{D}{d} = \frac{\lambda}{\alpha}, \tag{1}$$

where, $2\alpha = \frac{d}{D}$ is the aperture of the optical system.

To determine the axial extension of the bright spot, δz we consider a similar situation. δz in in comparison to the distance from the systems

aperture is small. Assume that we axially displace the observation plane from into to a parallel one. Similar to lateral directions in order to keep the axially displaced points in phase, therefore on a connected speckle grain, their path difference [1,2]:

$$\Delta = D - \delta z \cos\alpha - D + \delta z = \delta z(1 - \cos\alpha) = 2\delta z \sin^2 \frac{\alpha}{2} \tag{2}$$

should not exceed the wavelength, which gives:

$$\delta z \gg 2\frac{\lambda}{\alpha^2}, \tag{3}$$

which is taken as a measure of the axial dimension of the speckle grain. Hence, the speckle grains happen to be ellipsoids of typical dimensions δ and δz, as shown schematically in Fig. S2. Independent of the type of optical setup producing a speckle pattern, image formations, free space, or output of a multimode fiber, the typical dimensions of the speckles are determined by the wavelength and the aperture of the system and the diffraction is the physical phenomenon behind this.

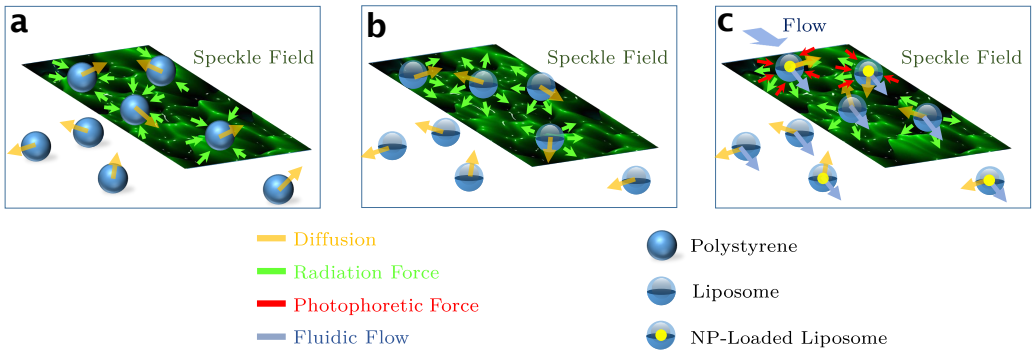

Supplementary Fig. S3: Schematic of the acting forces on (a) high refractive index particles, (a) low refractive index particles, and (c) nano-particle loaded low refractive index particles.

Schematic of the acting forces on various particles are shown in Fig. S3. The particles experience velocity changes over time while flowing in a particular high or low intensity region. The reason is the existence of multiple influential speckle grains that can avoid reaching a constant speed. The overall speed of a particle that passes through a speckle field is hindered, however, this happens in multiple interacting of the particle and the speckle field. Between each two steps their Brownian motion and varying optical (or photophoretic, in the case of NP-loaded liposomes) forces cause random motion so that they do not have sufficient free distance to reach to a constant speed. These concepts may be understood better by considering the information that Figs. 2 and 3 provide. The diffusion behavior of a particles in microscopic level can be better explained by considering the MSD vs. time curve. In the absence of an optical field, the particle is in normal diffusion regime and a linear behavior is resulted. In the presence of the

optical field, i.e., when the speckle field is on, in the initial times the particle still is in normal regime, but in longer times it falls in the subdiffusion regime. Increasing the mean intensity of the speckle field results in stronger subdiffusion behavior of the particles and the experiments show that this behavior is common between polystyrene, empty liposomes, and NP-loaded liposomes. However, the power in the power-law relation is lower in the case of NP-loaded liposomes, which is attributed to the presence of additional photophoretic forces. Photophoretic forces have a thermal origin and is effective in the optical manipulation of absorbing particles and may lead to spontaneous motion of them. These conclusions are deduced from power-law fitting to the data (Fig. 3) extracted from the measured trajectories (Fig. 2).

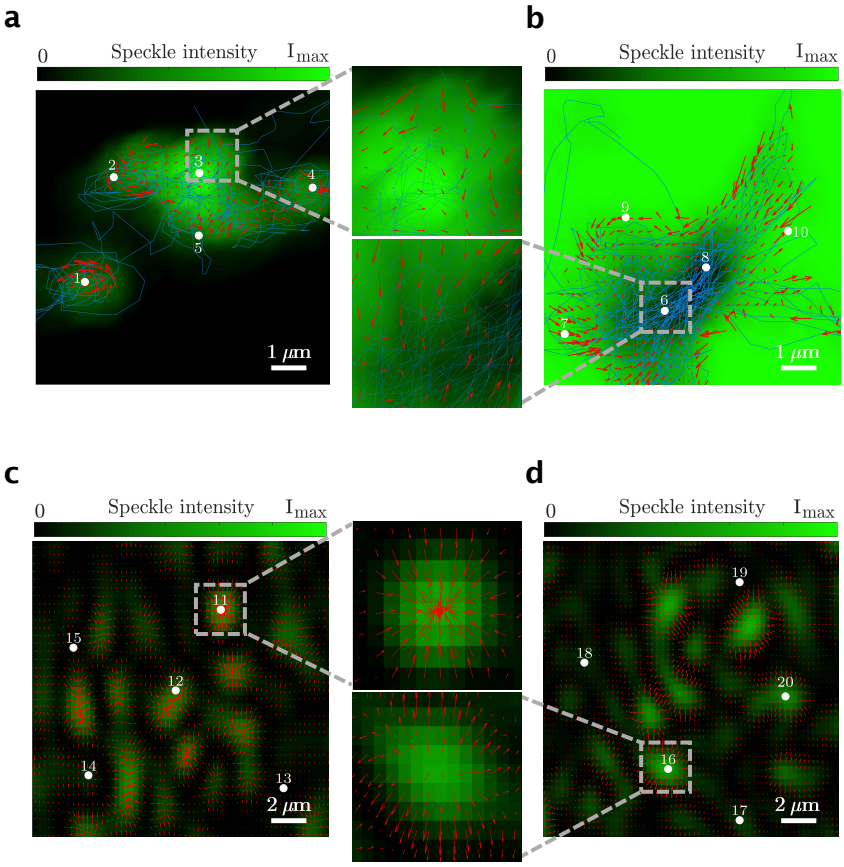

Supplementary Fig. S 4: Microscopic optical forces in a speckle field for (a) a polystyrene (high-refractive-index, $n_p = 1.59$) and (b) a liposome vesicle (low-refractive-index, $n_l = 1.30$), reconstructed through the analysis of particle displacement information via the maximum-likelihood-estimator analysis method. (c) and (d) The corresponding simulated force fields in speckle fields of the same average intensity as in (a) and (b). On each panel 5 randomly selected points are indicated whose quantitative optical potential values are presented in Table S5.

Table S1: Optical potential values of the randomly selected points on Fig. S4.

Number of point	U_x [K_BT] $\times 10^2$	U_y [K_BT] $\times 10^2$
1	0.0014	-0.0045
2	-0.0361	-0.029
3	-0.0085	-0.0115
4	-0.0346	-0.0126
5	-0.0869	-0.0229
6	-0.0552	-0.055
7	-0.0044	-0.0013
8	-0.028	-0.026
9	-0.0095	-0.0093
10	-0.0081	-0.0084
11	-0.00556	-0.00627
12	-0.00201	-0.00298
13	-0.0102	-0.0178
14	-0.00149	-0.00802
15	-0.0109	-0.0190
16	-0.00105	-0.00488
17	-0.00264	-0.00162
18	-0.00997	-0.00953
19	-0.00293	-0.00911
20	-0.00352	-0.001.69

References

[1] Joseph W Goodman, Speckle phenomena in optics: theory and applications (Roberts and Company Publishers, 2007).

[2] Rabal, Hector J., and Roberto A. Braga Jr, eds. Dynamic laser speckle and applications. CRC press, 2018.